

Title	Extensive study of giant magnetoresistance properties in half-metallic $\text{Co}_2(\text{Fe},\text{Mn})\text{Si}$ -based devices
Author(s)	Sakuraba, Y.; Ueda, M.; Miura, Y. et al.
Citation	Applied Physics Letters. 2012, 101(25), p. 252408
Version Type	VoR
URL	<a href="https://hdl.handle.net/11094/89406">https://hdl.handle.net/11094/89406</a>
rights	This article may be downloaded for personal use only. Any other use requires prior permission of the author and AIP Publishing. This article appeared in Y. Sakuraba, M. Ueda, Y. Miura, K. Sato, S. Bosu, K. Saito, M. Shirai, T. J. Konno, and K. Takanashi, "Extensive study of giant magnetoresistance properties in half-metallic $\text{Co}_2(\text{Fe},\text{Mn})\text{Si}$ -based devices", Appl. Phys. Lett. 101, 252408 (2012) and may be found at <a href="https://doi.org/10.1063/1.4772546">https://doi.org/10.1063/1.4772546</a> .
Note	

***Osaka University Knowledge Archive : OUKA***

<https://ir.library.osaka-u.ac.jp/>

Osaka University

## Extensive study of giant magnetoresistance properties in half-metallic Co<sub>2</sub>(Fe,Mn)Si-based devices

Y. Sakuraba, M. Ueda, Y. Miura, K. Sato, S. Bosu et al.

Citation: *Appl. Phys. Lett.* **101**, 252408 (2012); doi: 10.1063/1.4772546

View online: <http://dx.doi.org/10.1063/1.4772546>

View Table of Contents: <http://apl.aip.org/resource/1/APPLAB/v101/i25>

Published by the [American Institute of Physics](#).

---

### Related Articles

Anisotropic magnetoresistance in topological insulator Bi<sub>1.5</sub>Sb<sub>0.5</sub>Te<sub>1.8</sub>Se<sub>1.2</sub>/CoFe heterostructures  
*AIP Advances* **2**, 042171 (2012)

Angular-dependences of giant in-plane and interlayer magnetoresistances in Bi<sub>2</sub>Te<sub>3</sub> bulk single crystals  
*Appl. Phys. Lett.* **101**, 152107 (2012)

Magnetic field-dependent effective microwave properties of microwire-epoxy composites  
*Appl. Phys. Lett.* **101**, 152905 (2012)

Giant magnetoresistance effect in graphene with asymmetrical magnetic superlattices  
*Appl. Phys. Lett.* **101**, 152404 (2012)

Giant tunneling magnetoresistance in epitaxial Co<sub>2</sub>MnSi/MgO/Co<sub>2</sub>MnSi magnetic tunnel junctions by half-metallicity of Co<sub>2</sub>MnSi and coherent tunneling  
*Appl. Phys. Lett.* **101**, 132418 (2012)

---

### Additional information on *Appl. Phys. Lett.*

Journal Homepage: <http://apl.aip.org/>

Journal Information: [http://apl.aip.org/about/about\\_the\\_journal](http://apl.aip.org/about/about_the_journal)

Top downloads: [http://apl.aip.org/features/most\\_downloaded](http://apl.aip.org/features/most_downloaded)

Information for Authors: <http://apl.aip.org/authors>

## ADVERTISEMENT

**AIP** | Applied Physics  
Letters

**SURFACES AND INTERFACES**  
Focusing on physical, chemical, biological, structural, optical, magnetic and electrical properties of surfaces and interfaces, and more...

**ENERGY CONVERSION AND STORAGE**  
Focusing on all aspects of static and dynamic energy conversion, energy storage, photovoltaics, solar fuels, batteries, capacitors, thermoelectrics, and more...

**EXPLORE WHAT'S NEW IN APL**

**SUBMIT YOUR PAPER NOW!**

## Extensive study of giant magnetoresistance properties in half-metallic $\text{Co}_2(\text{Fe},\text{Mn})\text{Si}$ -based devices

Y. Sakuraba,<sup>1,a)</sup> M. Ueda,<sup>1</sup> Y. Miura,<sup>2</sup> K. Sato,<sup>1</sup> S. Bosu,<sup>1</sup> K. Saito,<sup>1</sup> M. Shirai,<sup>2</sup> T. J. Konno,<sup>1</sup> and K. Takanashi<sup>1</sup>

<sup>1</sup>Institute for Materials Research, Tohoku University, Katahira 2-1-1, Aoba-ku, Sendai 980-8577, Japan

<sup>2</sup>Research Institute of Electrical Communication (RIEC) and Center for Spintronics Integrated Systems (CSIS), Tohoku University, Katahira 2-1-1, Aoba-ku, Sendai 980-8577, Japan

(Received 12 November 2012; accepted 3 December 2012; published online 19 December 2012)

Fully epitaxial  $\text{Co}_2\text{Fe}_x\text{Mn}_{1-x}\text{Si}$ (CFMS)/Ag/ $\text{Co}_2\text{Fe}_x\text{Mn}_{1-x}\text{Si}$  current-perpendicular-to-plane giant magnetoresistive devices with various Fe/Mn ratios  $x$  and top CFMS layer thicknesses  $t_{\text{CFMS}}$  were prepared. The highest magnetoresistance (MR) ratios, 58% at room temperature and 184% at 30 K, were observed in the sample with  $x=0.4$  and  $t_{\text{CFMS}}=3$  nm. Enhancement of interface spin-asymmetry was suggested for  $x=0.4$  compared with that at  $x=0$ . A MR ratio of 58% was also observed even in a very thin trilayer structure, CFMS(4 nm)/Ag(3 nm)/CFMS(2 nm), which is promising for a next-generation magnetic read sensor for high-density hard disk drives. © 2012 American Institute of Physics. [<http://dx.doi.org/10.1063/1.4772546>]

The areal recording density of hard disk drives (HDDs) has increased markedly in the past two decades, reaching levels of the order of hundreds of gigabits per square inch. With regard to the development of magnetic read sensors for HDD, there have been innovative discoveries related to current-in-plane giant magnetoresistive (CIP-GMR) and tunneling magnetoresistive (TMR) effects.<sup>1–6</sup> Those present sensors based on MgO-based magnetic tunnel junctions (MTJs) cannot, however, be used for a higher areal density over 2 Tbit/in.<sup>2</sup> because the resistance-area product ( $RA$ ) of such a junction is too large. Current-perpendicular-to-plane giant magnetoresistive (CPP-GMR) devices are promising alternatives because they have a big advantage in keeping the  $RA$  small. Although a small MR ratio has a serious disadvantage of CPP-GMR devices used as read sensors, recent studies have shown that the MR ratio can be improved using half-metallic Heusler compounds.<sup>7–12</sup> We previously reported a large MR ratio for  $\text{Co}_2\text{MnSi}$ (CMS)/Ag/ $\text{Co}_2\text{MnSi}$  fully epitaxial CPP-GMR devices, 36% at room temperature (RT), which is an order of magnitude larger than that for conventional CPP-GMR devices using CoFe or NiFe.<sup>8,9</sup> We also found from first principles calculation on the transport in a (001)-CMS/Ag/CMS that not only half-metallicity but also the good matching of the majority-spin Fermi surfaces at the interface between (001)-oriented CMS and Ag (i.e., small interface resistance) is important for a high MR ratio.<sup>9</sup> Recently Sato *et al.* reported a very large MR ratio, 74.8% at RT, for  $\text{Co}_2\text{Fe}_{0.4}\text{Mn}_{0.6}\text{Si}$ /Ag/ $\text{Co}_2\text{Fe}_{0.4}\text{Mn}_{0.6}\text{Si}$  fully epitaxial CPP-GMR devices.<sup>12</sup> Although that was the largest MR ratio in CPP-GMR devices ever reported, it is still unclear how MR ratio,  $RA$ , and  $\Delta RA$  change when the composition and thickness of  $\text{Co}_2(\text{Fe},\text{Mn})\text{Si}$  (CFMS) electrodes vary. In addition, it is also important to understand the origin of the MR ratio enhancement due to substituting Fe for the Mn in CMS. In the present study, we

systematically investigated CPP-GMR properties in CFMS/Ag/CFMS devices of various compositions and thicknesses and also investigated the effect of measurement temperature.

Fully epitaxial CFMS/Ag/CFMS films were prepared by an ultrahigh-vacuum (UHV)-compatible magnetron sputtering system ( $P_{\text{base}} < 5 \times 10^{-8}$  Pa). First, Cr (20 nm) and Ag (40 nm) buffer layers were deposited on a MgO (001) single-crystal substrate at RT to improve the surface flatness. A 20-nm-thick lower CFMS layer was also grown at RT using a co-deposition technique with CMS and  $\text{Co}_2\text{FeSi}$  (CFS) alloy targets followed by *in situ* annealing at 500 °C to promote chemical ordering. After the sample was cooled to RT, a 5-nm-thick Ag spacer layer and an upper CFMS layer with a composition the same as that of the lower CFMS layer were deposited. Finally, the film was capped by Ag (2 nm) and Au (5 nm) protective layers. The Fe/Mn composition ratio  $x$  was set at either 0, 0.2, 0.3, 0.4, 0.5, or 1. The thickness of the upper CFMS layer ( $t_{\text{CFMS}}$ ) was varied from 3 to 10 nm. Films were patterned into a pillar shape for CPP-type four-terminal device structure using electron beam lithography and Ar ion milling. The designed size of pillars changed from  $50 \times 100$  to  $400 \times 800$  nm<sup>2</sup> (corresponding to  $120 \times 160$  to  $450 \times 820$  nm<sup>2</sup> in the actual pillar size  $A$  after Ar ion milling) on one substrate. In this study, we evaluated a parasitic electrode resistance  $R_{\text{para}}$  and  $RA$  by measuring the  $A$  dependence of device resistance  $R$ . Observed and intrinsic MR ratios are expressed as  $\text{MR}_{\text{obs}} = \Delta R / (R_{\text{P}}) \times 100(\%)$  and  $\text{MR}_{\text{int}} = \Delta R / (R_{\text{P}} - R_{\text{para}}) \times 100(\%)$ , respectively, where  $R_{\text{P}}$  is the resistance in the parallel state.

Figure 1(a) shows the XRD patterns for 50-nm-thick CFMS epitaxial films (on Cr/Ag buffer layers) with various  $x$  values. We found from the ratio of the intensity of the (002) superlattice peak to that of the (004) fundamental peak that all the CFMS films, regardless of  $x$ , had a (001)-oriented highly B2-ordered structure. The saturation magnetization ( $M_{\text{S}}$ ) measured by a vibrating sample magnetometer showed a systematic increase from 840 emu/cc for  $x=0.0$  to 1010 emu/cc for  $x=1.0$ . It was confirmed by an electron probe mass analysis

<sup>a)</sup>Author to whom correspondence should be addressed. Electronic mail: y.sakuraba@imr.tohoku.ac.jp. Tel.: +81-22-215-2097. Fax: +81-22-215-2096.

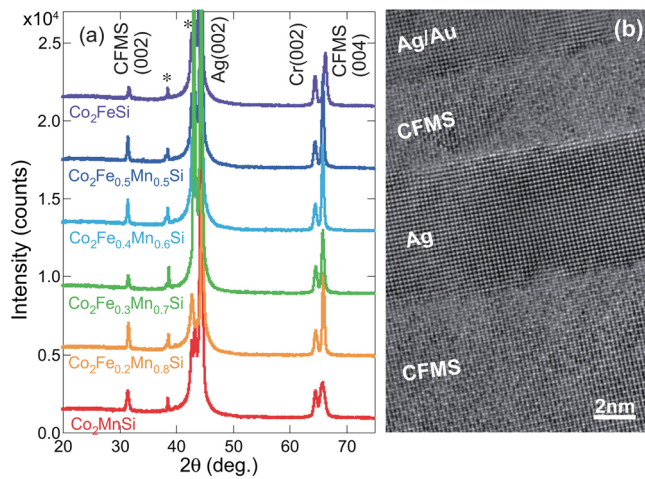


FIG. 1. (a) XRD patterns for CFMS at  $x$  from 0 to 1.0. (b) HRTEM image of the films with CFMS (20 nm,  $x=0.4$ )/Ag(5)/CFMS(3) structure. The peaks indicated with \* appearing at around  $38^\circ$  and  $42^\circ$  arise from the (002) diffraction from MgO substrate with Cu-K $\beta$  and K $\alpha$  sources, respectively.

that the actual Fe composition  $x$  in each film was almost the same as the designed value. As shown in Fig. 1(b), a high-resolution transmission electron microscope (HRTEM) image for a CFMS/Ag/CFMS ( $x=0.4$ ) film reveals a (001)-oriented fully epitaxial growth with very flat and sharp CFMS/Ag interfaces.

Figure 2 shows the Fe composition  $x$  dependence of the  $MR_{\text{int}}$  ratio of  $\text{Co}_2\text{Fe}_x\text{Mn}_{1-x}\text{Si}/\text{Ag}/\text{Co}_2\text{Fe}_x\text{Mn}_{1-x}\text{Si}$ . The thicknesses of the lower and upper CFMS layers were fixed at 20 and 7 nm, respectively. The inset shows the  $1/A$  dependence of the device resistance  $R$  for the sample with  $x=0.4$ . The parasitic resistance  $R_{\text{para}}$  and  $RA$  for each sample were estimated from the intercept and the slope, respectively, of the corresponding plot of  $R$  against  $1/A$ . We have confirmed an enhancement of the MR ratio with increasing  $x$  from CMS, and the highest  $MR_{\text{int}}$  ratio (46.7%) was obtained at  $x=0.4$  (with  $RA=23.7\text{ m}\Omega\mu\text{m}^2$  and  $\Delta RA=11.1\text{ m}\Omega\mu\text{m}^2$ ).

The upper CFMS thickness ( $t_{\text{CFMS}}$ ) dependence of  $MR_{\text{int}}$  ratio and  $\Delta RA$  was also investigated with  $x$  fixed at 0.4 and

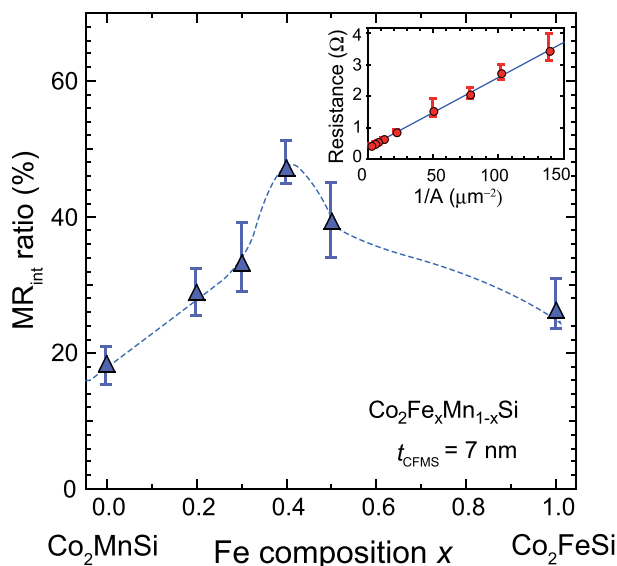


FIG. 2. Fe composition dependence of  $MR_{\text{int}}$  ratio in CFMS(20)/Ag(5)/CFMS(7) CPP-GMR devices.

at 0, which are shown in Figs. 3(a) and 3(b). There is no remarkable  $t_{\text{CFMS}}$  dependence of  $\Delta RA$  from 3 to 10 nm thick for both  $x=0$  and 0.4, indicating that the spin-diffusion length of CFMS ( $\lambda_{\text{CFMS}}$ ) is less than 3 nm, which is similar to the result obtained for  $\text{Co}_2\text{FeAl}_{0.5}\text{Si}_{0.5}$ (CFAS)/Ag/CFAS ( $\lambda_{\text{CFAS}} \sim 2.2\text{ nm}$ ).<sup>10</sup> The highest  $MR_{\text{int}}$  and  $MR_{\text{obs}}$  (58% and 49%) were obtained at  $t_{\text{CFMS}}=3\text{ nm}$  for  $x=0.4$ .

Here, an effect of substituting Fe for the Mn in  $\text{Co}_2\text{MnSi}$  will be discussed. There are several first-principle calculations on the DOS in CFMS.<sup>13–16</sup> Some of them claimed half-metallicity in CFS<sup>15,16</sup> but the others predicted the disappearance of half-metallicity in CFS because  $E_{\text{F}}$  comes into the conduction band of the half-metallic gap.<sup>13,14</sup> Previous studies on MTJs, magnetic damping factors, and AMR showed that the half-metallicity of CFMS disappears when  $x$  becomes greater than 0.6–0.8.<sup>13,14</sup> It was also suggested from the measurements of Hall effect and x-ray circular dichroism that  $E_{\text{F}}$  shifts towards the conduction band by substituting Fe for Mn in the  $\text{Co}_2\text{MnSi}$ .<sup>17,18</sup> The decrease of MR ratio from  $x=0.4$  in Fig. 2 can, therefore, be understood by the intrinsic change of electronic states in CFMS with changes in  $x$ , i.e., the spin polarization gradually decreases with  $x$ . On the other hand, the enhancement of MR ratio at  $x$  from 0 to 0.4 is difficult to be explained by a change of DOS with  $x$ . In order to clarify this point, we consider a variation of the bulk and interface spin-asymmetry coefficients,  $\beta$  and  $\gamma$ , from  $x=0$  to 0.4. Generally,

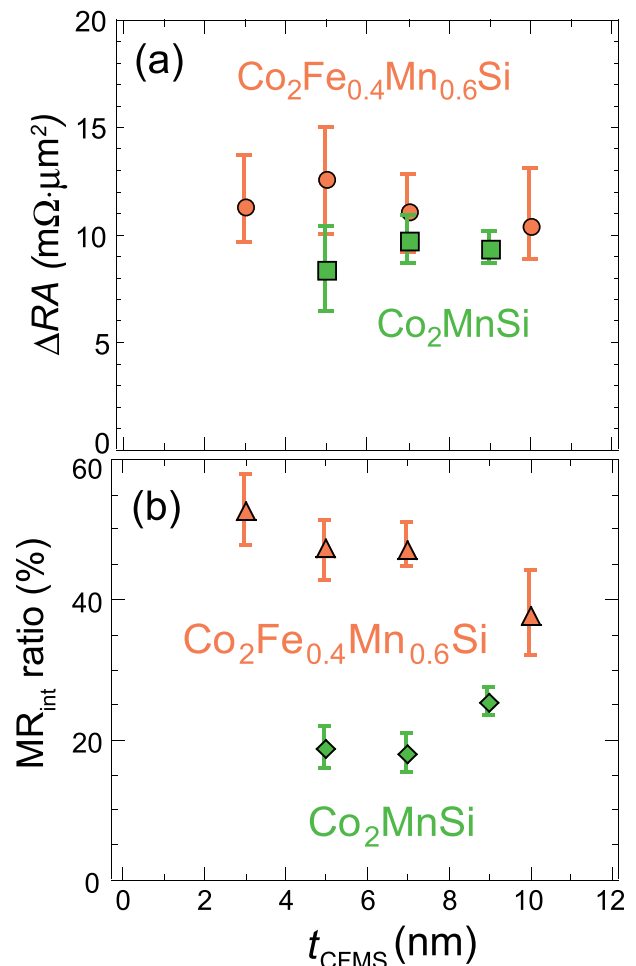


FIG. 3. The  $t_{\text{CFMS}}$  dependence of (a)  $\Delta RA$  and (b)  $MR_{\text{int}}$  ratio in CFMS(20 nm)/Ag/CFMS( $t_{\text{CFMS}}$ ) with  $x=0$  and 0.4.



it is possible to evaluate  $\beta$  and  $\gamma$  from the analysis for the ferromagnetic layer thickness dependence of  $\Delta RA$  using the two-current model.<sup>19</sup> Although the quantitative analyses of  $\beta$  and  $\gamma$  have not been completed in this study because we could not observe clear reduction of  $\Delta RA$  even at  $t_{\text{CFMS}} = 3$  nm, it is predicted that  $\gamma$  is improved from  $x = 0$  to 0.4 by comparing  $\Delta RA$  between  $x = 0$  and 0.4. In the two-current-model for the CPP-GMR staking structure,<sup>19</sup>  $\Delta RA$  is proportional to  $(\beta\rho_{\text{CFMS}}^*t_{\text{CFMS}} + \gamma R_{\text{CFMS/Ag}}^*A)^2$  when  $t_{\text{CFMS}}$  is thinner than  $\lambda_{\text{CFMS}}$  and saturated after  $t_{\text{CFMS}}$  becomes thicker than  $\lambda_{\text{CFMS}}$ . Here,  $\rho_{\text{CFMS}}^*$  is the resistivity of CFMS  $\rho_{\text{CFMS}}$  divided by  $(1 - \beta^2)$  and  $R_{\text{CFMS/Ag}}^*$  is the interface resistance  $R_{\text{CFMS/Ag}}$  divided by  $(1 - \gamma^2)$ . It was observed in the CFMS single-layer film that the  $\rho_{\text{CFMS}}$  at  $x = 0.4$  was  $46 \mu\Omega \text{ cm}$ , which was slightly higher than that at  $x = 0.0$ ,  $37 \mu\Omega \text{ cm}$ . Nevertheless, the  $RA$  for  $\text{Co}_2\text{Fe}_{0.4}\text{Mn}_{0.6}\text{Si}/\text{Ag}/\text{Co}_2\text{Fe}_{0.4}\text{Mn}_{0.6}\text{Si}$  was smaller than that for  $\text{CMS}/\text{Ag}/\text{CMS}$  (at  $t_{\text{CFMS}} = 5$  nm,  $RA \sim 24 \text{ m}\Omega \mu\text{m}^2$  for  $\text{Co}_2\text{Fe}_{0.4}\text{Mn}_{0.6}\text{Si}$  and  $31 \text{ m}\Omega \mu\text{m}^2$  for  $\text{CMS}$ ), which indicated that  $R_{\text{CFMS/Ag}}$  is smaller at  $x = 0.4$  than at  $x = 0$ . The observed  $\Delta RA$  at  $x = 0.4$  is clearly larger than that at  $x = 0$  (at  $t_{\text{CFMS}} = 5$  nm,  $\Delta RA \sim 11\text{--}12 \text{ m}\Omega \mu\text{m}^2$  for  $\text{Co}_2\text{Fe}_{0.4}\text{Mn}_{0.6}\text{Si}$  and  $8 \text{ m}\Omega \mu\text{m}^2$  for  $\text{CMS}$ ). Therefore, these results suggest that  $\gamma$  at the CFMS/Ag was enhanced from  $x = 0$  to 0.4.

Furthermore, in order to investigate a possible mechanism of the enhancement of  $\gamma$  from  $x = 0$  to 0.4, we also performed the first-principles calculations of the exchange stiffness of Co spin-moment at the Co-terminated CMS/Ag and CFS/Ag interfaces using the quantum code ESPRESSO.<sup>20</sup> We constructed multilayer CMS/Ag and CFS/Ag structures containing seventeen atomic layers of CMS or CFS and nine atomic layers of Ag with the Co termination. Other parameters of the first-principles calculations are shown in Ref. 21. To estimate the exchange stiffness of the interfacial Co spin-moments in CMS/Ag and CFS/Ag, we calculated the increase of the one-electron band energy  $E(\theta)$  as a function of the tilting angle of the local spin moments  $\theta$  in the non-collinear spin system. Then, we fitted these results using  $E(\theta) = A(1 - \cos \theta)$ , where  $A$  is the inter-atomic-layer exchange stiffness constant. It was found from our first-principles calculations that the exchange stiffnesses of Co at the Co-terminated CMS/Ag and CFS/Ag interfaces are, respectively, 137 and 340 meV. This behavior of the exchange stiffness at interfacial regions can be attributed to a large Co spin moment in CFS/Ag ( $1.16 \mu_B$ ) as compared with that in CMS/Ag ( $0.72 \mu_B$ ), because the exchange stiffness constant is related to local spin moments.<sup>21</sup> As is discussed in Ref. 22, the total magnetic moment of bulk  $\text{Co}_2\text{Fe}_x\text{Mn}_{1-x}\text{Si}$  follows the Slater-Pauling behavior  $M = Z - 24$ , where  $M$  is the total spin moment in  $\mu_B$  per unit cell and  $Z$  is the total number of valence electrons, which scales linearly with the Fe concentration  $x$ . In this case, it is energetically more favorable that the Co spin moment in bulk CFS is increased as compared with that in bulk CMS because of charge transfer from the Co minority-spin states to the Fe minority-spin states.<sup>21</sup> Thus, the interfacial Co spin moment of CFS/Ag is also larger than that of CMS/Ag, leading to the strong exchange stiffness of Co spin moment in CFS/Ag as compared with that in CMS/Ag. The Co-termination at the CFMS/Ag interface was experimentally confirmed from a scanning transmission electron microscopy image.<sup>12</sup> Therefore, one possible origin for the increase of MR ratio as  $x$  increases

from 0 to 0.4 is the improvement of interfacial exchange stiffness of Co at the Ag spacer, which results in the enhancement of  $\gamma$  at RT as suggested from this study.

The temperature dependence of  $\text{MR}_{\text{obs}}$  ratio in the sample with  $t_{\text{CFMS}} = 3$  nm and  $x = 0.4$  is shown in Fig. 4. The maximum  $\text{MR}_{\text{obs}}$  and  $\text{MR}_{\text{int}}$  (165% and 184%) were obtained at 30 K. The origin of the reduction of MR ratio below 30 K is still unclear, but similar behaviors in CMS/Ag/CMS have been reported before.<sup>23,24</sup> It was suggested in Ref. 23 that the MR reduction in a low temperature (LT) region could have been due to Mn atoms that diffused from CMS layers into the Ag spacer and created a spin-glass state of Mn moments that degraded spin-dependent transport in the LT region. On the other hand, it was also proposed in Ref. 24 that the presence of bi-quadratic interlayer exchange coupling in CMS/Ag/CMS caused the reduction of MR ratio in a LT region. The temperature dependence of the MR ratio normalized by that at 300 K is shown in the inset of Fig. 4 for the CFMS/Ag/CFMS with  $x = 0.0, 0.3, 0.5,$  and 1. It is clear that the temperature where the MR ratio shows the maximum gradually decreases with  $x$ . That is, CFS/Ag/CFS shows no reduction of MR ratio in a LT-region, implying the presence of Mn and its amount are important for the MR reduction in a LT-region.

In order to use a CPP-GMR device in a magnetic read sensor for next-generation HDDs with storage densities over 5 Tbit/in.<sup>2</sup>, the total thickness of the device will need to be less than 10.5 nm.<sup>25</sup> We, therefore, also investigated a MR property in a thinner CFMS/Ag/CFMS ( $x = 0.4$ ) trilayer structure. We have fabricated a very thin structure with CFMS(4 nm)/Ag(3 nm)/CFMS(2 nm) and observed a large  $\text{MR}_{\text{obs}}$  ( $\text{MR}_{\text{int}}$ ) ratio of 43% (58%) with  $RA = 21.7 \text{ m}\Omega \mu\text{m}^2$  (Fig. 5). This result suggests a strong contribution of interfacial spin-dependent scattering to the MR ratio in this system, which facilitates the use of this system in a magnetic read sensor of HDD because it means that we can decrease total device thickness while maintaining a high MR.

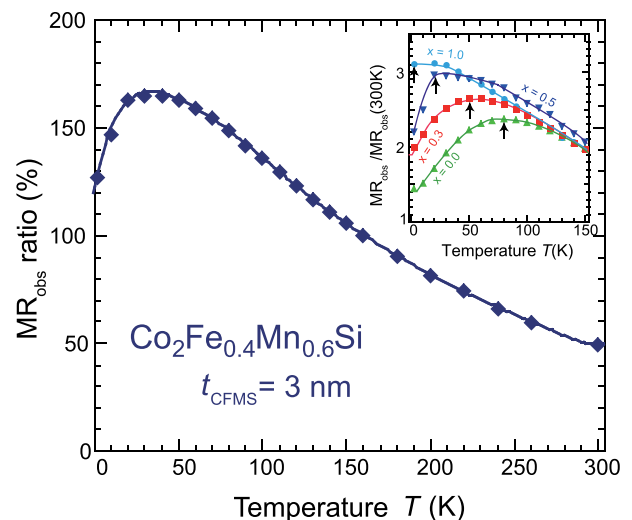


FIG. 4. Temperature dependence of  $\text{MR}_{\text{obs}}$  ratio for the sample with CFMS(20 nm)/Ag/CFMS(3 nm,  $x = 0.4$ ) structure. The inset shows temperature dependence of  $\text{MR}_{\text{obs}}$  ratio normalized by that at 300 K for the samples with  $x = 0.0, 0.3, 0.5,$  and 1.0. The arrows indicate the highest MR ratio observed in each sample.

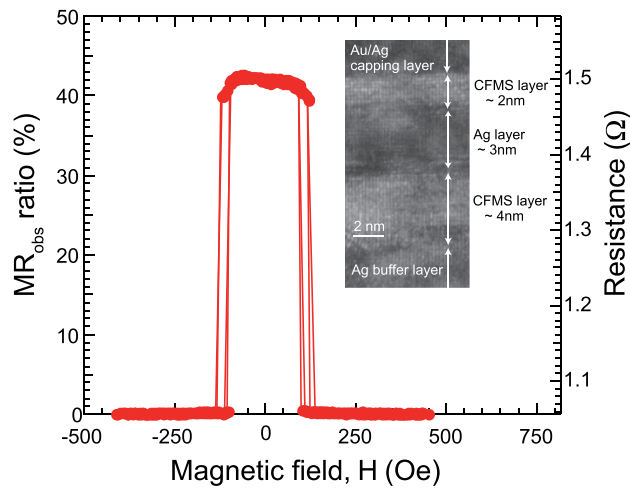


FIG. 5. MR curve for the sample with a CFMS(4 nm)/Ag(3 nm)/CFMS(2 nm) structure at RT. The inset shows a HR-TEM image of the sample.

In conclusion, in this study, we fabricated  $\text{Co}_2\text{Fe}_x\text{Mn}_{1-x}\text{Si}/\text{Ag}/\text{Co}_2\text{Fe}_x\text{Mn}_{1-x}\text{Si}$  fully epitaxial CPP-GMR devices, systematically changing the Fe/Mn composition ratio  $x$  and the CFMS electrode thickness  $t_{\text{CFMS}}$ . The highest intrinsic MR ratios, 58% at RT and 184% at 30 K, were observed in the device with  $x = 0.4$  and  $t_{\text{CFMS}} = 3$  nm. It was suggested by comparing  $\Delta RA$  between  $x = 0$  and 0.4 that the interface spin-asymmetry  $\gamma$  was improved in the  $\text{Co}_2\text{Fe}_{0.4}\text{Mn}_{0.6}\text{Si}/\text{Ag}$ . It was revealed from our first-principles calculation on the exchange stiffness of Co spin moment at the Co-terminated CMS/Ag and CFS/Ag interfaces that the interfacial exchange stiffness of Co improved with increasing  $x$ , which was one possible origin of the enhancement of MR ratio at  $x$  from 0 to 0.4. A large intrinsic MR ratio of 58% was also observed even in a very thin trilayer structure—CFMS(4 nm)/Ag(3 nm)/CFMS(2 nm)—because of the large interface contribution to MR, which is promising for magnetic read sensors in the next-generation HDDs.

The authors thank T. M. Nakatani, N. Hase, Y. K. Takahashi, and K. Hono for useful discussions, and Y. Kodama for the help in TEM specimen preparation using FIB. This work was supported by the Strategic International Cooperative Program ASPIMATT from JST and Storage Research Consortium (SRC). This work was a part of the cooperative research program of ARCMG, Institute for Materials Research, Tohoku University.

- <sup>1</sup>P. Grunberg, R. Schreiber, Y. Pang, M. B. Brodsky, and H. Sowers, *Phys. Rev. Lett.* **57**, 2442 (1986).
- <sup>2</sup>M. N. Baibich, J. M. Brot, A. Fert, F. Nguyen Van Dau, F. Petroff, P. Eitenne, G. Creuzet, A. Friederich, and J. Chazelas, *Phys. Rev. Lett.* **61**, 2472 (1988).
- <sup>3</sup>T. Miyazaki and N. Tezuka, *J. Magn. Magn. Mater.* **139**, L231 (1995).
- <sup>4</sup>S. Yuasa, T. Nagahama, A. Fukushima, Y. Suzuki, and K. Ando, *Nature Mater.* **3**, 868 (2004).
- <sup>5</sup>S. S. P. Parkin, C. Kaiser, A. Panchula, P. M. Rice, B. Hughes, M. Samant, and S. H. Yang, *Nature Mater.* **3**, 862 (2004).
- <sup>6</sup>D. D. Djayaprawira, K. Tsunekawa, M. Nagai, H. Maehara, S. Yamagata, N. Watanabe, S. Yuasa, Y. Suzuki, and K. Ando, *Appl. Phys. Lett.* **86**, 092502 (2005).
- <sup>7</sup>K. Yakushiji, K. Saito, S. Mitani, K. Takanashi, Y. K. Takahashi, and K. Hono, *Appl. Phys. Lett.* **88**, 222504 (2006).
- <sup>8</sup>T. Iwase, Y. Sakuraba, S. Bosu, K. Saito, S. Mitani, and K. Takanashi, *Appl. Phys. Express* **2**, 063003 (2009).
- <sup>9</sup>Y. Sakuraba, K. Izumi, Y. Miura, K. Futasukawa, T. Iwase, S. Bosu, K. Saito, K. Abe, M. Shirai, and K. Takanashi, *Phys. Rev. B* **82**, 094444 (2010).
- <sup>10</sup>T. M. Nakatani, T. Furubayashi, S. Kasai, H. Sukegawa, Y. K. Takahashi, S. Mitani, and K. Hono, *Appl. Phys. Lett.* **96**, 212501 (2010).
- <sup>11</sup>Y. K. Takahashi, A. Srinivasan, B. Varaprasad, A. Rajanikanth, N. Hase, T. M. Nakatani, S. Kasai, T. Furubayashi, and K. Hono, *Appl. Phys. Lett.* **98**, 152501 (2011).
- <sup>12</sup>J. Sato, M. Oogane, H. Naganuma, and Y. Ando, *Appl. Phys. Express* **4**, 113005 (2011).
- <sup>13</sup>T. Kubota, S. Tsunegi, M. Oogane, S. Mizukami, T. Miyazaki, H. Naganuma, and Y. Ando, *Appl. Phys. Lett.* **94**, 122504 (2009).
- <sup>14</sup>F. J. Yang, Y. Sakuraba, S. Kokado, Y. Kota, A. Sakuma, and K. Takanashi, *Phys. Rev. B* **86**, 020409(R) (2012).
- <sup>15</sup>S. Wurmehl, G. H. Fecher, H. C. Kandpal, V. Ksenofontov, H.-J. Lin, J. Morais, and C. Felser, *Phys. Rev. B* **72**, 184434 (2005).
- <sup>16</sup>H. C. Kandpal, G. H. Fecher, G. Schönhense, and C. Felser, *Phys. Rev. B* **73**, 094422 (2006).
- <sup>17</sup>H. Schneider, E. Vilanova Vidal, S. Chadov, G. H. Fecher, C. Felser, and G. Jakob, *J. Magn. Magn. Mater.* **322**, 579–584 (2010).
- <sup>18</sup>M. Kallmayer, P. Klaer, H. Schneider, E. Arbelo Jorge, C. Herbort, G. Jakob, M. Jourdan, and H. J. Elmers, *Phys. Rev. B* **80**, 020406R (2009).
- <sup>19</sup>T. Valet and A. Fert, *Phys. Rev. B* **48**, 7099 (1993).
- <sup>20</sup>P. Giannozzi, S. Baroni, N. Bonini, M. Calandra, R. Car, C. Cavazzoni, D. Ceresoli, G. L. Chiarotti, M. Cococcioni, I. Dabo, A. Dal Corso, S. Fabris, G. Fratesi, S. de Gironcoli, R. Gebauer, U. Gerstmann, C. Gougoussis, A. Kokalj, M. Lazzeri, L. Martin-Samos, N. Marzari, F. Mauri, R. Mazzarello, S. Paolini, A. Pasquarello, L. Paulatto, C. Sbraccia, S. Scandolo, G. Sclauzero, A. P. Seitsonen, A. Smogunov, P. Umari, and R. M. Wentzcovitch, *J. Phys.: Condens. Matter* **21**, 395502 (2009).
- <sup>21</sup>Y. Miura, K. Abe, and M. Shirai, *Phys. Rev. B* **83**, 214411 (2011).
- <sup>22</sup>I. Galanakis, P. H. Dederichs, and N. Papanikolaou, *Phys. Rev. B* **66**, 174429 (2002).
- <sup>23</sup>Y. Sakuraba, K. Izumi, S. Bosu, K. Saito, and K. Takanashi, *J. Phys. D: Appl. Phys.* **44**, 064009 (2011).
- <sup>24</sup>H. S. Goripati, M. Hayashi, T. Furubayashi, T. Taniguchi, H. Sukegawa, Y. K. Takahashi, and K. Hono, *J. Appl. Phys.* **110**, 123914 (2011).
- <sup>25</sup>M. Takagishi, K. Yamada, H. Iwasaki, H. N. Fuke, and S. Hashimoto, *IEEE Trans. Magn.* **46**, 2086 (2010).